Int J Adv Manuf Technol
DOI 10.1007/s00170-012-3980-z

ORIGINAL ARTICLE

Multi-objective process optimization for micro-end milling of Ti-6Al-4V titanium alloy

Thanongsak Thepsonthi · Tuğrul Özel

Received: 20 June 2011 / Accepted: 6 February 2012

Abstract Micro-end milling is one of the promising methods for rapid fabrication of features with 3D complex shapes. However, controlling the micro-end milling process to obtain the desired results is much harder compared to that of macro-end milling due to the size effect and uncontrollable factors. The problem is much pronounced when workpiece material is a difficult-to-process material such as titanium-based alloys which are widely used as material of choice for aircraft structures, turbine blades, and medical implants. In order to find the optimal process parameters which minimize the surface roughness and burr formation, experiments were conducted and models obtained with statistically based methods utilized in multi-objective particle swarm optimization to identify optimum process parameters. The results show that the average surface roughness can be minimized while burr formation is reduced concurrently.

Keywords Micro-end milling · Titanium alloy · Process optimization · Response surface methodology · Particle swarm optimization

1 Introduction

Mechanical micromachining process or tool-based micromachining process is one of manufacturing processes which is now gaining a lot of attention from many industries. Since the process is capable of fabricating miniature parts as small as tens micrometers to a few millimeters with very complex features and close tolerances using energy-efficient small machine tools [14, 22]. The major advantage of mechanical micromachining processes compared to the other processes used in fabrication of miniature parts is the process flexibility. Since there is no limitation in machining shape, many complex features such as 3D cavities and arbitrary curvatures, or a high aspect ratio feature such as long shafts and micro-channels can be achieved. Also, the setup cost of mechanical micromachining process is very low and the material removal rate is higher compared to its counterparts such as micro-electro-mechanical system (MEMS)-based methods. Thus, it is very suitable for a small batch production or even a custom-made product. In addition, mechanical micromachining has no limitation in terms of type of workpiece materials, unlike most of the MEMS-based processes which are limited to a few silicon-based materials.

Micro-end milling is the most flexible process among all mechanical micromachining processes. Its capabilities provide many advantages for manufacturing of complex features, especially those in medical devices and implants. However, scaling the conventional milling process down to a microscale results in encountering several problems. Many factors that can be ignored in macroscale become significant in microscale; for instance, vibration, deflection, temperature, microstructure of workpiece, etc. As a result, obtaining the desired performances in micro-end milling is more difficult than that of macro-end milling [8, 11, 30, 31, 36]. This problem is even more elevated when workpiece materials are difficult-to-process materials such as titanium alloys which are generally used in medical devices and implants.

Titanium-based alloys are very suitable for medical applications due to their high strength-to-weight ratio, corrosion resistance, and biocompatibility. Since the potential for

T. Thepsonthi · T. Özel (✉)
Manufacturing & Automation Research Laboratory, Department of Industrial and Systems Engineering, Rutgers University, Piscataway, NJ 08854, USA
e-mail: ozel@rutgers.edu

Published online: 31 March 2012

micro-parts as medical tools operating at cellular level is increasing [25], research into the micromachining of titanium alloys is gaining more interest. The challenge in machining titanium alloys is chiefly the high tool wear associated with the reactivity of titanium with tool materials and its low thermal conductivity [15]. Moreover, studies in gaining understanding of micromachining titanium alloys are still limited. Therefore, it is difficult for the industry to successfully implement this process.

Controlling of machined surface in micro-end milling is regarded as a technological challenge in micro-end milling since surface topography of micro-features is in a sub-micrometer order and it is very difficult to treat these micro-features with finishing processes. The topography of machined surface fundamentally affects functional performance of the micro-product in terms of friction, lubrication, etc. For example, it has been reported that micro-milling of titanium alloy for medical applications especially for implants can create free-form surfaces, which can improve biocompatibility [32, 33]. Therefore, in order to produce functional micro-products, not only part features and tolerances have to be concerned but surface quality must be considered as well. Several approaches have been used in order to gain a control over the surface finish of micro-features; for example, process parameters optimization [39], surface generation modeling and simulation [10, 21, 23, 38], effects of using lubrication [17, 24], etc.

In micromachining, burr formation is another critical problem on surface finish. Burr formation depends principally on the workpiece material in terms of ductility, cutter geometry, cutting parameters, tool wear, and shape of workpiece [3, 4, 27]. Burrs also frequently occur when micromachining hard materials due to increased tool wear [40]. Moreover, deburring and surface finishing or micro-features are limited due to expensive techniques or the resulting damages on the microstructures [13]. Many studies on micro-milling have shown that burr formation is very difficult to avoid; however, selecting appropriate process parameters and tool geometry can minimize the effect to an acceptable level [2, 6, 20, 34]. In recent studies, slip-line field analysis is utilized to model plastic deformation in micro-end milling to understand size effects and force generation [16].

In order to improve the surface quality of micro-features, both surface roughness and burr formation should be considered and controlled together. Since both are process parameter dependent, optimality of one may result in an unaccepted outcome of another. Therefore, the objectives of this work were to explore a performance of micro-end milling of Ti-6Al-4V titanium alloy and optimize the process parameters in order to improve the surface quality in terms of surface roughness and burr formation [31].

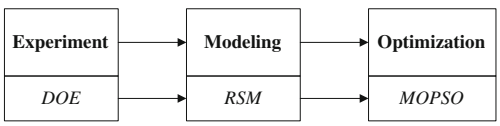

Fig. 1 Work flow and methods utilized

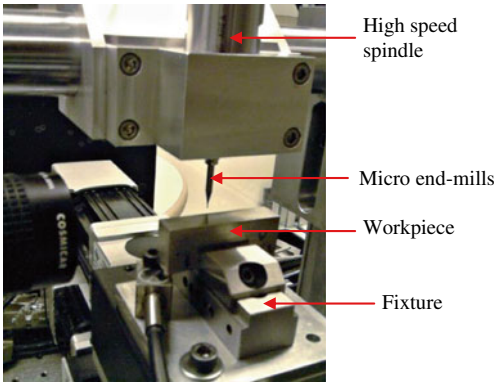

Fig. 2 The experimental setup

2 Methodology

This work consists of three phases: experiment, modeling, and optimization. The first phase, experimental phase, was where the physical micro-milling experiments were conducted in order to collect all necessary data in measured surface roughness and burr formation. The main method in this phase was a design of experiment using Taguchi orthogonal arrays. In the second phase, modeling phase, all data obtained in the experimental phase were used to formulate the predictive process models. In this phase, the response surface methodology (RSM) was used to construct the

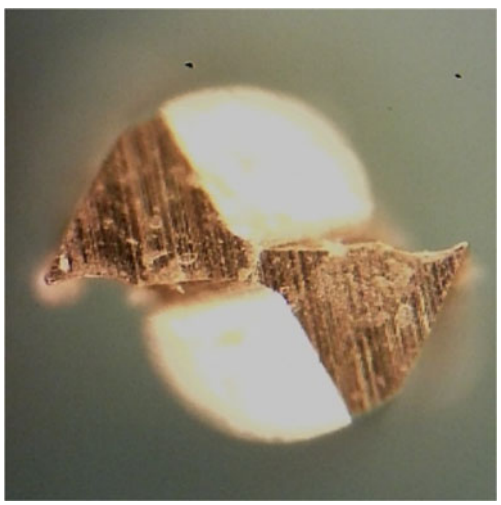

Fig. 3 The bottom view of the micro-end mill

Table 1 Parameters and levels assigned for the experiments

Factor	Micro-milling parameters	Levels		
		−1	0	1
Ω	Spindle speed (krpm)	20	40	60
f_z	Feed per tooth (μm/tooth)	0.1	0.3	0.5
ADOC	Axial depth of cut (μm)	20	60	100

predictive models. Finally, the last phase, optimization phase, was carried out in order to obtain the optimal parameters that satisfy the multi-criteria quality requirement. The multi-objective particle swarm optimization (MOPSO) was selected as an optimization method for this phase. The work flow and tools used in each phase are shown in Fig. 1.

2.1 Experimental

A rectangular block Ti-6Al-4V titanium alloy workpiece was clamped on the fixture mounted on the table of the in-house developed four-axis micro-end milling machine. The workpiece surfaces were precisely ground to assure flatness and alignment. The fine grain carbide (grain size of 0.2–0.5 μm) two-flute flat bottom end mills with the diameter of 0.025″ (0.635 mm), helix angle of 30°, length of cut of 0.0375″, and the mean edge radii of 3±0.5 μm were selected. The tool was mounted directly to the ceramic bearing electrically driven precision spindle (NSK ASTRO-E 800) with the tool overhang of 18 mm. Figure 2 shows the experimental setup.

The full-immersion slot micro-end milling of 12-mm straight grooves (channels) was conducted with various levels of cutting parameters. All grooves/channels were machined without any coolant or lubricant. Figure 3 shows the micro-end mill.

Table 2 Taguchi L9 orthogonal array with three factors and three levels and run order for each replication

Standard	Run order		Factors and their levels		
Run	Rep. I	Rep. II	Ω (krpm)	f_z (μm/tooth)	ADOC (μm)
1	1	9	20	0.1	20
2	2	8	20	0.3	60
3	7	3	20	0.5	100
4	3	7	40	0.1	60
5	4	6	40	0.3	100
6	8	2	40	0.5	20
7	5	5	60	0.1	100
8	6	4	60	0.3	20
9	9	1	60	0.5	60

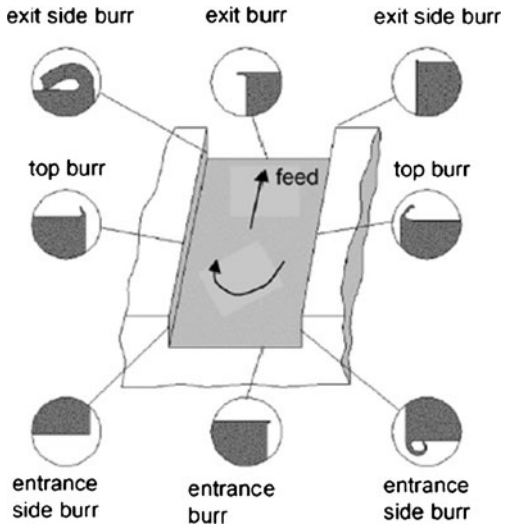

Fig. 4 Types of milling burrs [12]

In order to determine cutting parameters affecting the performance of micro-end milling of Ti-6Al-4V titanium alloy as well as to find an optimal cutting condition which results in the best surface roughness and minimal burr formation, an experimental design based on Taguchi method was applied with three-factor three-level design. The tested parameters included spindle speed (Ω in thousand revolutions per minute), feed per tooth (f_z in micrometer per tooth) and axial depth of cut (ADOC, in micrometers). The L9 orthogonal array was selected for an experiment of three process parameters with three levels. Each experimental run was replicated twice with a different experimental order. Fresh micro-end mills were used for each replication. Despite a very short machined length, tool condition was inspected with digital microscopy after completion of each replication and tool wear was found negligible. Table 1 shows the parameters and their levels employed in the experimental run. Table 2 shows Taguchi L9 orthogonal array design with three factors and three levels and experimental run order for each replication.

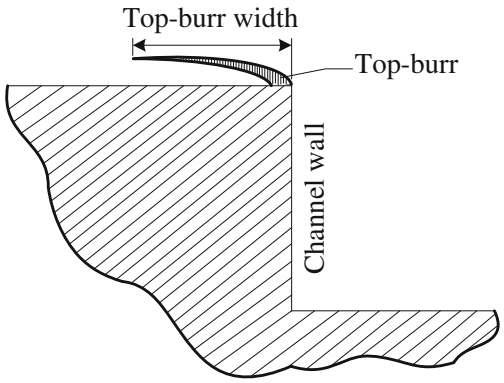

Fig. 5 Definition of top burr width

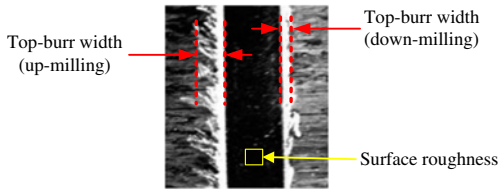

Fig. 6 Measurement locations for the micro-channels

In every experimental run, the responses were measured in terms of average surface roughness (R_a) and total top burr width. The surface roughness measurements were taken from three different locations along the bottom of the channel using Mitutoyo SJ-400 digital surface analyzer, and the average value was recorded.

In a milling process, there are several types of burr formed at different locations based on direction of cutting and contact of workpiece and the micro-end mill. In this study, a special focus was given to the top burr formation which is a dominant burr mechanism in groove/channel milling. Top burr is one of the burr types that occur during the end milling process. It is defined as a burr attached to the top surface of the workpiece. The top burr is generated by a minor cutting edge with a side flow formation [3, 4]. Types of milling burrs are shown in Fig. 4 as adopted from [12].

To quantitatively measure a degree of top burr formation, a term top burr width was defined as a horizontal length of burr from the channel wall. Figure 5 illustrates the measurement of top burr width. The top burr width was measured by using digital microscopy. Three measurements were taken from three different locations where burr length is uniform. Since the full immersion was used in this groove/channel milling, the channel side walls were machined with different approaches; one side wall was machined with down milling, while the other was machined with up milling.

The difference of up/down milling yielded a difference degree of top burr formation. Thus, the term total top burr width was defined as a summation of top burr widths measured from up milling side and top burr widths measured from down milling side. Measurement locations of surface roughness and top burr width are shown in Fig. 6.

2.2 Process modeling

In order to optimize the parameters of micro-milling process, it is necessary to construct relationships between the response and each interested process parameter. One of the well-known methods serving this purpose is RSM.

RSM is a collection of mathematical and statistically based technique useful for the modeling and analysis of problems with several process variables. It also has important applications in the design, development, and formulation of new products, as well as in the improvement of existing product designs [28].

The most extensive applications of RSM are in the situation where several input variables (independent variable) are potentially influencing some performance measure or quality characteristic of the product or process (response). Since the form of the relationship between the response and the independent variable is unknown, the first step in RSM is to find the suitable approximation for the true functional relationship between response (y) and the set of independent variables (x).

Usually a low-order polynomial in some relatively small region of the independent variable space provides a suitable approximation of the true form of the response function. In many cases, either a first-order or a second-order model is sufficient. The general form of the first-order, first-order with interaction, and second-order RSM model are shown in Eqs. 1, 2, and 3, respectively, where β is a RSM

Table 3 Summary of the experimental results

Run	Factors and levels			R_a (μm)		Top burr width (mm)					
						Up milling		Down milling		Total	
	Ω	f_z	ADOC	Rep. I	Rep. II	Rep. I	Rep. II	Rep. I	Rep. II	Rep. I	Rep. II
1	20	0.1	20	0.257	0.263	0.147	0.175	0.075	0.115	0.222	0.290
2	20	0.3	60	0.140	0.113	0.210	0.271	0.110	0.106	0.320	0.377
3	20	0.5	100	0.107	0.150	0.157	0.148	0.068	0.047	0.225	0.195
4	40	0.1	60	0.180	0.163	0.125	0.182	0.061	0.079	0.186	0.261
5	40	0.3	100	0.153	0.157	0.132	0.168	0.057	0.064	0.189	0.232
6	40	0.5	20	0.100	0.117	0.220	0.194	0.103	0.086	0.323	0.280
7	60	0.1	100	0.163	0.150	0.078	0.050	0.054	0.044	0.132	0.094
8	60	0.3	20	0.153	0.163	0.236	0.199	0.075	0.053	0.311	0.252
9	60	0.5	60	0.127	0.110	0.117	0.082	0.069	0.050	0.186	0.132

coefficient of each term, k is a number of independent variables, and $\in$ is a residual error.

$$y = \beta_0 + \sum_{i=1}^{k} \beta_i x_i + \in \quad (1)$$

$$y = \beta_0 + \sum_{i=1}^{k} \beta_i x_i + \sum_{i<j} \sum \beta_{ij} x_i x_j + \in \quad (2)$$

$$y = \beta_0 + \sum_{i=1}^{k} \beta_i x_i + \sum_{i<j} \sum \beta_{ij} x_i x_j + \sum_{i=1}^{k} \beta_{ii} x_i^2 + \in \quad (3)$$

The first-order model is sometimes called a main effect model because it includes only the main effect of the variables. If there is an interaction between these variables, the interaction terms can be easily added as shown in Eq. 2. Adding the interaction terms introduces curvature into the response function. If the curvature in the true response surface is strong enough that the first-order model (even with the interaction terms included) is inadequate, a second-order model will be required.

The second-order model is widely used in RSM for several reasons. First, the second-order model is very flexible; it can take on a wide variety of functional forms. Second, an estimation of the coefficient (β) can be done easily by the method of least squares. Furthermore, there is considerable practical experience indicating that the second-order works well in solving real response surface problem [29]. In this study, surface roughness (R_a) and total top burr width were selected as responses while spindle speed (ohms), feed per tooth (f_z), and axial depth of cut (ADOC) were independent variables. The experimental results obtained from the first phase were used to formulate the RSM models for each response.

2.3 Process optimization

Typically, it appears that the relationship between machining parameters and machining responses is nonlinear, which is sometimes very difficult to optimize analytically. The problem becomes even more difficult when there is a need to optimize more than one objective at a time (i.e., multi-objective optimization). Multi-objective optimization problems represent an important class of real-world problems. Typically, such problems involve trade-offs meaning that their objectives are generally conflicting to each other. For example, mold manufacturers may want to obtain minimum surface roughness, but meanwhile they also want to minimize the machining time. Generally, there is no single optimal solution. Therefore "trade-off" has to be considered before choosing the suitable solution. The curve or surface (for more than two objectives) describing the optimal trade-off solutions between objectives is known as the Pareto front. A multi-objective optimization algorithm is required to find solutions as close as possible to the Pareto front while maintaining good solution diversity along the Pareto front.

In this study, the MOPSO was selected since it has many advantages over other optimization methods. It works very efficiently to locate the Pareto front of the multi-objective optimization problems. Also, it is relatively easy to implement and has a few parameters to adjust.

In general, Particle Swarm Optimization (PSO) is a population-based stochastic optimization technique modeled on the social behaviors observed in animals or insects, e.g., bird flocking, fish schooling, and animal herding. PSO was developed by Kennedy and Eberhart in 1995 [19]. Since its inception, PSO has gained increasing popularity among researchers and practitioners as a robust and efficient technique for solving difficult optimization problems.

In PSO, individual particles of a swarm represent potential solutions, which move through the variable space seeking an optimal, or good enough, solution. The particles relay

Table 4 Response table for the mean surface roughness (in micrometers)

Factor	Level 1	Level 2	Level 3	Max–min	Rank
Ω	0.172	0.145	0.144	0.027	3
f_z	0.196	0.147	0.119	0.078	1
ADOC	0.176	0.139	0.147	0.037	2

Table 5 Response table for the mean total top burr width (in millimeters)

Factor	Level 1	Level 2	Level 3	Max–min	Rank
Ω	0.27	0.25	0.18	0.087	2
f_z	0.20	0.28	0.22	0.083	3
ADOC	0.28	0.24	0.18	0.102	1

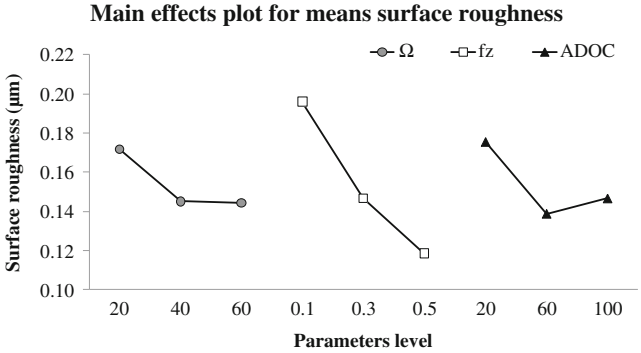

Fig. 7 Main effects plot for the mean surface roughness

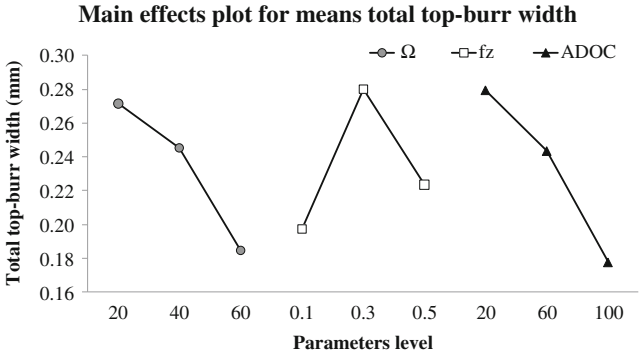

Fig. 8 Main effects plot for the mean total top burr width

their current positions to neighboring particles. The position of a particle is modified by using its previous position information and its current velocity (i.e., rate of change). As the model is iterated, the swarm focuses more and more on an area of the search space containing high-quality solutions [5].

In PSO, the velocity of each particle is modified iteratively by its personal best position (i.e., the best position found by the particle so far) and the best position found by particles in its neighborhood. As a result, each particle searches around a region defined by its personal best position and the best position from its neighborhood.

$$v_i^{k+1} = wv_i^k + c_1R_1\left(p_i - x_i^k\right) + c_2R_2\left(p_g - x_i^k\right) \tag{4}$$

$$x_i^{k+1} = x_i^k + v_i^{k+1} \tag{5}$$

Where v_i^k denotes the velocity of the ith particle at kth iteration in the swarm, x_i^k denotes its current position which can be considered as a set of coordinates describing a point in space, p_i denotes the personal best position, p_g denotes the best position found by particles in its neighborhood, w denotes an inertia weight, c_1 and c_2 are acceleration coefficients, and R_1 and R_2 are two separate functions each returning a vector comprising random values uniformly generated in the range (0, 1).

Equation 4 shows that the velocity term v_i^k of a particle is determined by three parts, the "momentum," the "cognitive," and the "social" part. The "momentum" term wv_i^k represents the weighted ratio of previous velocity term which is used to carry the particle in the direction it has traveled so far; the "cognitive" part, $c_1R_1\left(p_i - x_i^k\right)$, represents the tendency of the particle to return to the best position it has visited so far; the "social" part, $c_2R_2\left(p_g - x_i^k\right)$, represents the tendency of the particle to be attracted towards the position of the best position found by the entire swarm. The random numbers used in the velocity update step give the PSO a stochastic behavior. It should be noted that the "momentum" term has a tendency to explode to a large value, resulting in particles exceeding the boundaries of the search space. This is more likely to happen especially when a particle is far from p_g or p_i. To overcome this problem, a velocity clamping method can be adopted where the maximum allowed velocity value is set to $V_{\max}$ in each dimension of v_i [9, 35].

Position p_g in the "social" part is the best position found by particles in the neighborhood of the ith particle. Different neighborhood topologies can be used to control information propagation between particles. Constricted information propagation as a result of using small neighborhood topologies has been shown to perform better on complex problems, whereas larger neighborhoods generally perform better on simpler problems [26].

Generally speaking, a PSO implementation that chooses p_g from within a restricted local neighborhood is referred to as *lbest* PSO, whereas choosing p_g without any restriction (hence from the entire swarm) results in a *gbest* PSO.

Algorithm below summarizes a basic PSO algorithm.

- Initial step: Randomly generate an initial swarm position and velocities. The current position of each particle is set as p_i. The p_i with the best value is set as p_g.

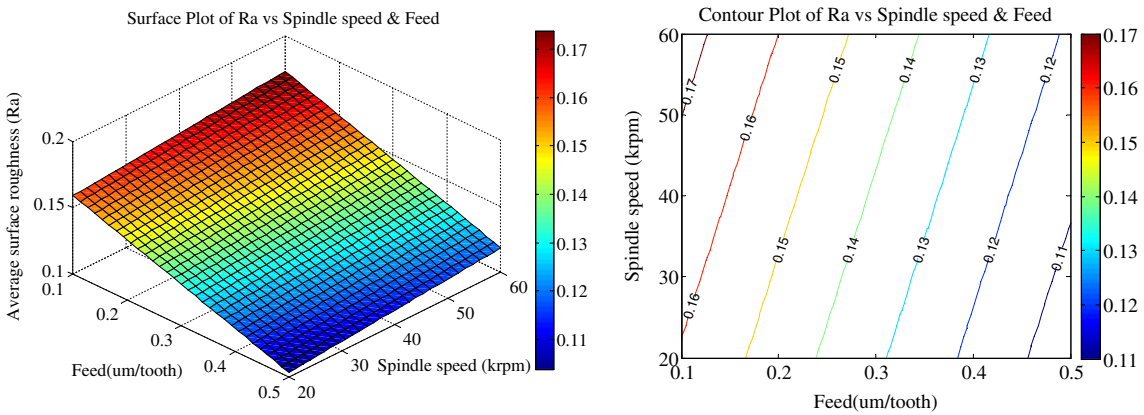

Fig. 9 Surface and contour plots of average surface roughness (ohms in thousand revolutions per minute vs. f_z in micrometers per tooth)

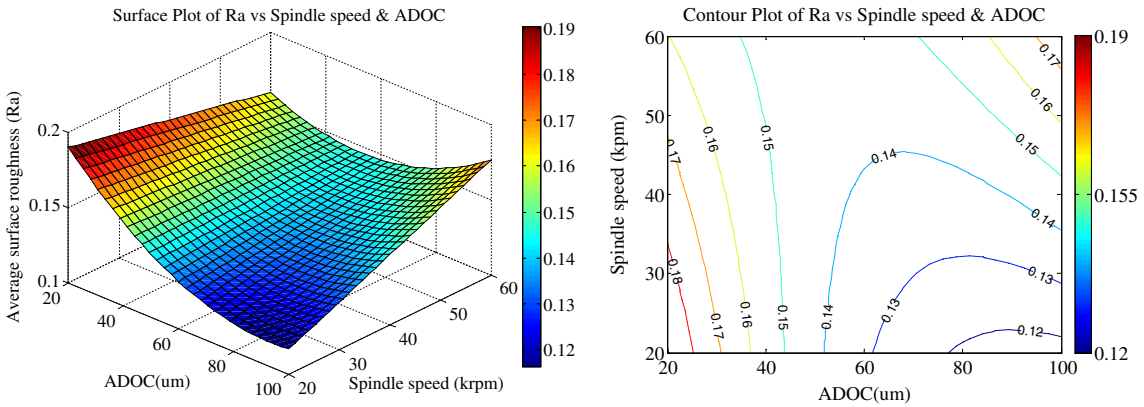

Fig. 10 Surface and contour plots of average surface roughness (ohms in thousand revolutions per minute vs. ADOC in micrometers)

- Step 1: For each particle, the objective function value is evaluated. If an agent achieves a better objective value, p_i is replaced by the current position x_i.
- Step 2: Set p_g equal to the best collected p_i values.
- Step 3: Update the velocity by Eq. 4 and update the position by Eq. 5.
- Step 4: Return to step 1 and repeat until the termination criterion is met.

PSO algorithms have been applied to optimization problems ranging from classical problems such as scheduling, the traveling salesman problem, neural network training, and task assignment, to highly specialized applications. In recent years, PSO has also become a popular choice for many researchers in handling multi-objective optimization problems in manufacturing processes [7, 18, 37].

In this study, MOPSO methodology proposed by Alvarez-Benitez et al. [1] is adopted. The selection of global guides (p_g) is based on Pareto dominance. An external archive is used to store the non-dominated solutions found by the algorithm. When new non-dominated solutions are found, they are entered into the archive, and existing members of the archive are deleted if they are dominated by the new solutions. The idea is to select a global guide for a particle from the archive members that dominate the particle. One particle can be dominated by more than one non-dominated solution. The selection can be made randomly or a promotion value can be assigned to each non-dominated solution which increases with the number of iterations. An archive member with high promotion value is more likely to be picked as a global guide. After an archive member is selected, its promotion value is reset to zero. In addition, the archive members in densely populated regions are more likely to dominate more particles than the archive members in sparsely populated regions.

The MOPSO algorithm was implemented in MATLAB, the RSM models formulated from the previous phase served as objective functions, *f(x)* and *g(x)*. After completion of the MOPSO algorithm, the Pareto frontier was located indicating a set of solutions in the multi-objective domain. Moreover, all solutions were plotted in a variables domain showing the optimal level of each parameter.

3 Results and discussions

Results and discussion are divided into three parts which are related to the experimental phase described earlier. These

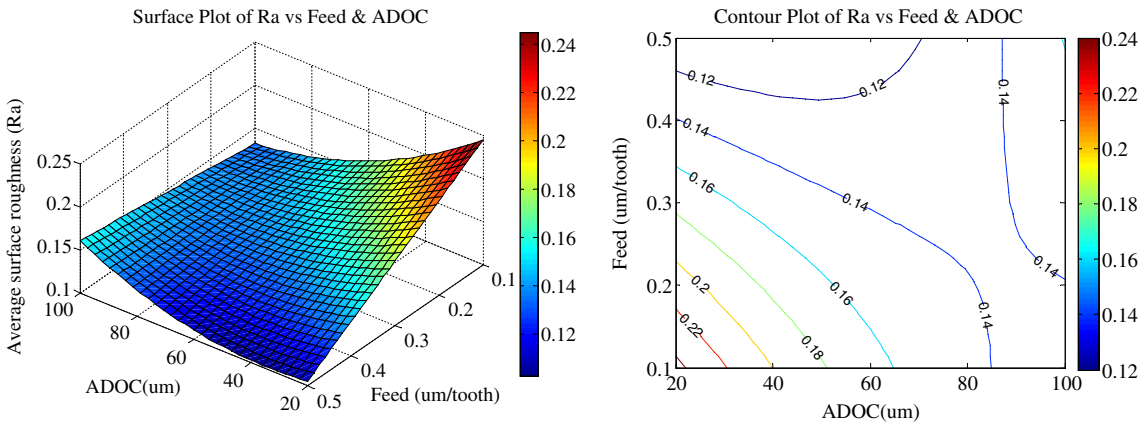

Fig. 11 Surface and contour plots of average surface roughness (f_z in micrometers per tooth vs. ADOC in micrometers)

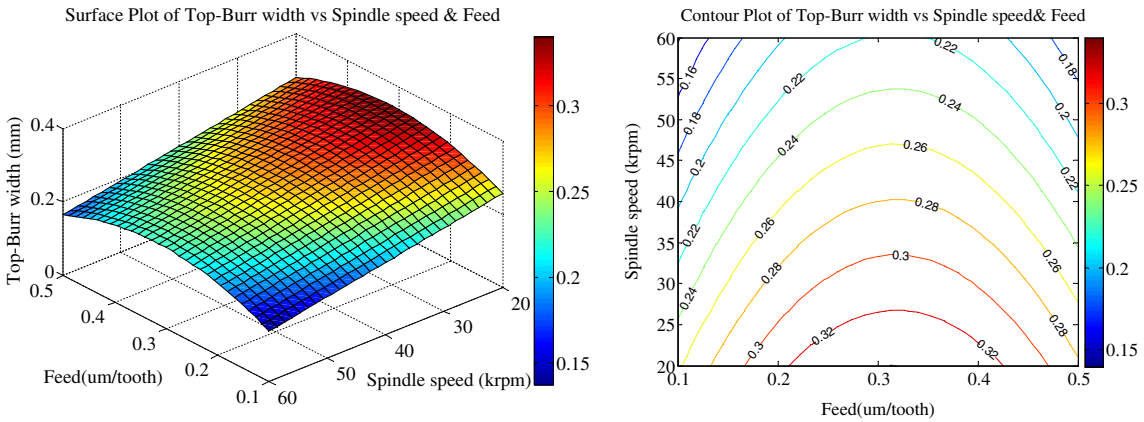

Fig. 12 Surface and contour plots of top burr width (ohms in thousand revolutions per minute vs. f_z in micrometers per tooth)

three parts consist of experimental results, modeling results, and multi-objective optimization results.

3.1 Experimental results

Table 3 shows all results from the experiment, while Tables 4 and 5 show the analysis of means for surface roughness and total top burr width, respectively. Figures 7 and 8 illustrate the main effects for surface roughness and total top burr width, respectively. In terms of surface roughness (R_a), it can be seen that the main effect of feed per tooth (f_z) is ranked number one among all the three factors and the effect is approximately twice of the other. This indicates the dominated influence over the surface roughness of the feed per tooth. It shows that increase feed per tooth results in decrease of surface roughness. The influence of each tested parameters over the total top burr width is not significantly different. The axial depth of cut (ADOC) seems to have a slightly higher effect than the other two factors. In addition, it is quite obvious that the top burr width from up milling is larger than those from down milling (see Table 4).

In summary, both surface roughness and top burr formation are parameter-dependent. Based on the experimental results, setting spindle speed and feed per tooth at high levels and axial depth of cut at medium level yields the lowest surface roughness, and setting spindle speed and axial depth of cut at high level and feed per tooth at low level yields minimum total top burr width. However, these settings are not the same, meaning that obtaining the best result for both performance measurements is not possible. One performance has to be sacrificed in order to attain another. Therefore, using the multi-objectives optimization technique would be very helpful for this difficult decision making.

3.2 Modeling results

Based on the experimental result in Table 2, the second-order RSM models for both responses, top burrs width and surface roughness, were formulated. The estimated regression coefficients were obtained using the method of least square. Equation 6 represents the RSM model for surface roughness, and Eq. 7 represents the RSM

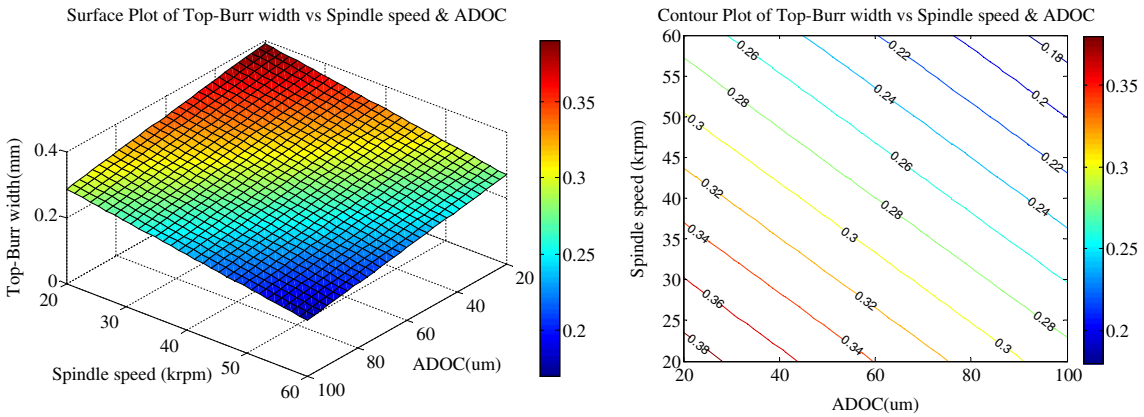

Fig. 13 Surface and contour plots of top burr width (ohms in thousand revolutions per minute vs. ADOC in micrometers)

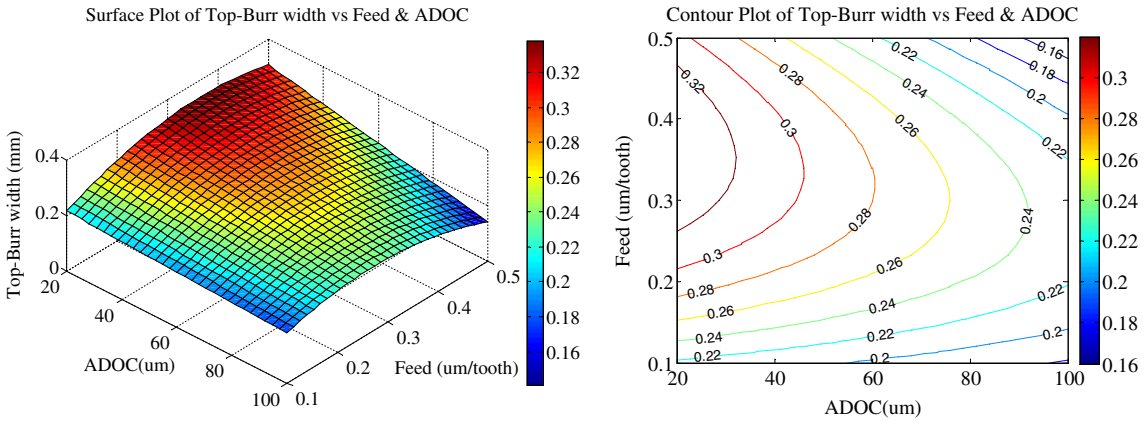

Fig. 14 Surface and contour plots of top burr (f_z in micrometers per tooth vs. ADOC in micrometers)

model for top burr width. Please note that the analysis was done using coded unit and the models only include the significant terms.

$$R_a = 0.13883 + 0.00729\,A - 0.02762B - 0.01442C + 0.02225C^2 + 0.02226AC + 0.04190BC \quad (6)$$

$$\text{Total top} - \text{burr width} = 0.28017 - 0.0593\,A + 0.013B - 0.05092\,C - 0.06967B^2 - 0.0316BC \quad (7)$$

Since the analysis was done using coded units, the variables A, B, and C were given as coded variable and can be calculated by using Eqs. 8, 9, and 10, respectively, where Ω is a spindle speed (thousand revolutions per minute), f_z is a feed per tooth (micrometers per tooth), and ADOC is an axial depth of cut (micrometers)

$$A = \frac{\Omega - 40}{20} \quad (8)$$

$$B = \frac{f_z - 0.3}{0.2} \quad (9)$$

$$C = \frac{\text{ADOC} - 60}{40} \quad (10)$$

To measure model adequacy, R^2, predicted R^2, and adjusted R^2 were calculated. For the surface roughness model, R^2, predicted R^2, and adjusted R^2 were found to be 93.55%, 82.78%, and 90.03%, respectively, and for the top burr width model, these values were found to be 82.91%, 62.95%, and 75.79%, respectively. Since both models obtained satisfactory

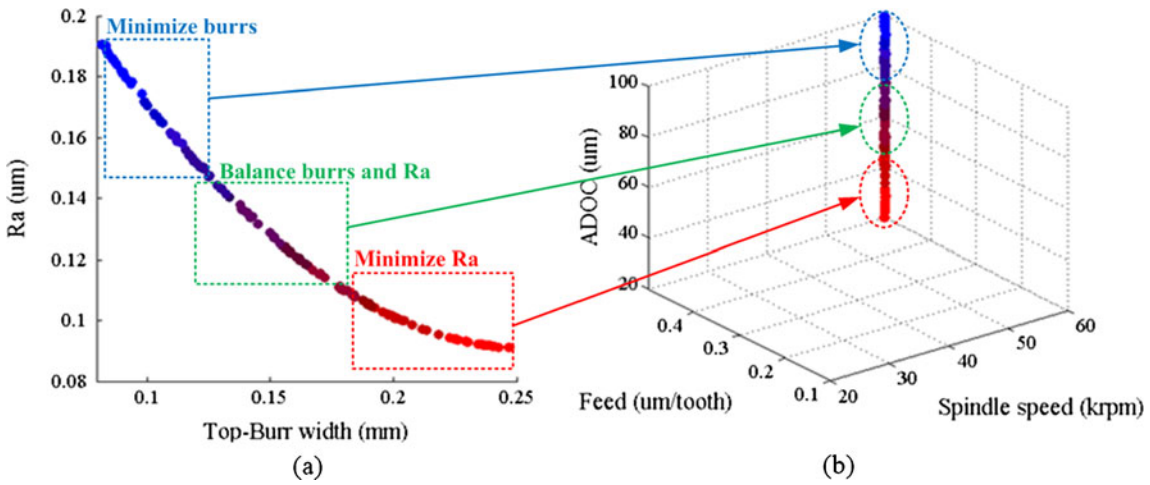

Fig. 15 MOPSO results (**a**) Pareto front of optimal objective value (**b**) optimal solution in variable domain

high value of all R^2, the models are well fitted to the real data points.

Using the developed RSM models, the surface plots and contour plots of each model were created. An extra parameter in the surface plots was held at the middle level. The surface and contour plots of the average surface roughness against process parameters are shown in Figs. 9, 10, and 11, while the surface and contour plots of total top burr width against process parameters are shown in Figs. 12, 13, and 14.

It should be noted that there are some conflicts in terms of recommended parameter levels obtained from the main effects plots (Figs. 7 and 8) and those obtained from the surface plots. This can be explained by the fact that the main effect analysis is a quick and simple experimental analysis which only considers the influence of each factor individually and does not concern any interaction or squared effects. Its purpose was to quickly capture an effect of the factors to the responses. On the other hand, the RSM models included all interaction and squared effects, and in this study, it has been shown that these effects are significant.

3.3 Results of multi-objective optimization

In this study, since there is a trade-off between surface roughness and burr formation, a multi-objective optimization becomes necessary. Finding the optimal process parameters to achieve the desired level of response (minimum average surface roughness and minimum burr formation) can be performed.

Multi-objective optimization problem with two objective functions can be formulated as following:

$$\begin{aligned} &\text{Minimize}\{f(x), g(x)\} \\ &\text{s.t.} \quad f(x) \le b_1 \\ &\qquad g(\mathbf{x}) \le b_2 \\ &\qquad x \in X \end{aligned} \tag{11}$$

where x represent micro-milling process parameters; $x = x_1, x_2, ..., x_n$ $(x_1 = \Omega, x_2 = f_z, x_3 = \text{ADOC})$. X represents the solution space with all feasible values for the micro-milling process parameters. The function $f(x)$ represents the objective function for surface roughness, and the function $g(x)$ represents the objective function for total top burr width. b_1 and b_2 are upper bound of $f(x)$ and $g(x)$, respectively

The simulations are run by using a particle swarm population of 250 and a maximum number of 500 iterations with varying learning rates. After obtaining the best particle value in each iteration of the simulation, the particles are plotted in a two-dimensional objective space for viewing. This procedure is repeated until a clear Pareto frontier forms. The simulations usually take less than 30 min in a PC with Intel Dual-Core 2.40 GHz processor. Therefore, the Pareto frontiers of the non-dominated solution sets are obtained by using this multi-objective PSO method.

The Pareto frontier of the non-dominated solutions for two objective functions minimizing surface roughness, min (R_a), and minimizing total top burr width, min (top burr width), is presented in Fig. 15a. Micro-milling process parameters that minimize both top burr width and surface roughness are identified along the ADOC axis at the highest

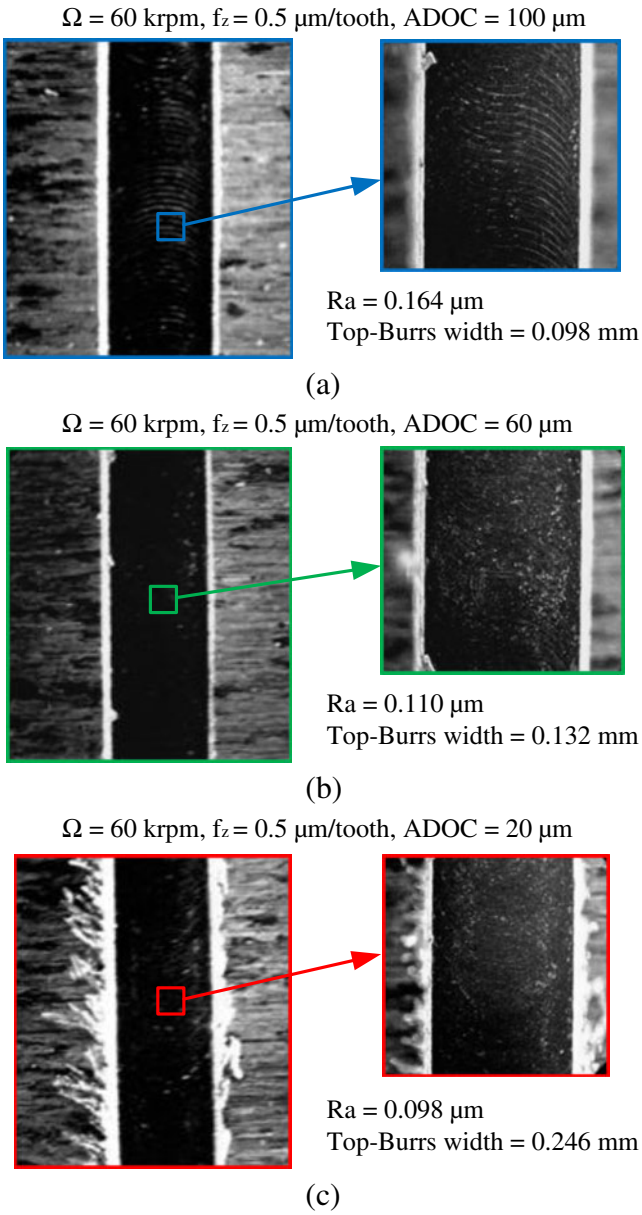

Fig. 16 Examples of channel quality based on the result from MOPSO (**a**) channel with minimum top burrs width (**b**) channel with balanced top burrs and surface roughness (**c**) channel with minimum surface roughness

spindle speed tested (60 krpm) and at the highest feed per tooth (50 μm) in the solution (decision variable) space (see Fig. 15b).

Three distinct regions have been identified along the Pareto frontier of the non-dominated solution set in Fig. 15a. These are marked as "minimize burrs," "balance burrs and surface roughness," and "Minimize Ra." Corresponding regions in the solution (decision variable) space are also indicated in Fig. 15b. A set of micro-end milling process parameters falling in these regions should provide decision maker (operator) a feasible solution set to achieve desired surface roughness and total top burr width.

In addition, optimum process parameters that satisfy both objective functions in minimizing surface roughness and top burr width are utilized in a set of experiments. At first, a set of process parameters is employed (Ω=60 krpm, f_z=0.5 μm/tooth, and ADOC=100 μm) which is found optimum for obtaining minimum top burr width as shown in Fig. 16a. Another set is employed in micro-end milling a channel with set (Ω=60 krpm, f_z= 0.5 μm/tooth, and ADOC=60 μm) which is determined to be an optimum set for minimizing both surface roughness and top burr width equally as shown in Fig. 16b. Finally, another set of optimum process parameters for minimizing surface roughness only (Ω=60 krpm, f_z=0.5 μm/tooth, and ADOC=20 μm) is utilized in Fig. 16c. As it is evident from the validation experiments, the smaller the ADOC, larger the top burr width.

4 Conclusions

In this work, a process modeling and optimization for micro-end milling of Ti-6Al-4V titanium alloy has been performed by using experimental, statistically based modeling and particle swarm optimization methods. The application of statistically based methods was proven to be useful for obtaining the optimal process parameters for a desired surface quality. Particle swarm optimization method for multi-criteria process parameter selection in micro-end milling has also proven to be a successful approach. The following is a summary of other important findings:

- Axial depth of cut is found to be the major process parameter causing top burr formation.
- Feed per tooth or feed rate is found to be the major process parameter affecting surface roughness. However, in contrast with conventional milling, a higher feed rate provides a better surface roughness and channel quality.
- Achieving a high surface roughness and minimum burr formation is highly dependent upon an achievable axial depth of cut and feed rate which also results in a high productivity.
- The approach and the methodologies employed in this work can be utilized in optimizing micromachining of other materials using micro-manufacturing processes.

References

1. Alvarez-Benitez JE, Everson RM, Fieldsend JE (2005) A MOPSO algorithm based exclusively on pareto dominance concepts, Proceedings of Third International Conference on Evolutionary Multi-Criterion Optimization, Guanajuato, Mexico
2. Aramcharoen A, Mativenga PT (2009) Size effect and tool geometry in micromilling of tool steel. Precis Eng 33(4):402–407
3. Aurich JC, Dornfeld D, Arrazola PJ, Franke V, Leitz L, Min S (2009) Burrs-analysis, control and removal. CIRP Ann Manuf Technol 58(2):519–542
4. Aurich JC, Dornfeld D, Arrazola PJ, Franke V, Leitz L, Min S (2009) Burrs: analysis, control and removal. CIRP Annals Manuf Technol 58:519–542
5. Blum C, Li X (2008) Swarm intelligence in optimization. In: Blum C, Merkel D (eds) Swarm intelligence introduction and applications. Springer, Berlin, pp 58–62
6. Chern GL, Wu YJE, Cheng JC, Yao JC (2007) Study on burr formation in micro-machining using micro-tools fabricated by micro-EDM. Precis Eng 31(2):122–129
7. Ciurana J, Arias G, Özel T (2009) Neural network modeling and particle swarm optimization of process parameters in pulsed laser micro-machining of hardened AISI H13 steel. Mater Manuf Process 24:358–368
8. Dhanorker A, Özel T (2008) Meso/micro scale milling for micro-manufacturing. Int J Mechatron Manuf Syst 1(1):23–43
9. Eberhart RC, Shi Y (2001): Particle swarm optimization: developments, applications and resources. Proc. Congress on Evolutionary Computation 2001, Seoul, Korea. Piscataway, NJ: IEEE Service Center.
10. Elkaseer AM, Popov K B, Negm M, Dimov SS, Minev R (2010) Material micro structure effect-based simulation model for the surface generation process in micro-milling, *ICOMM/4 M 2010*, April, 2010; Madison, Wisconsin.
11. Filiz S, Conley CM, Wasserman MB, Ozdoganlar OB (2007) An experimental investigation of micro-machinability of copper 101 using tungsten carbide micro-endmills. Int J Mach Tool Manuf 47:1088–1100
12. Hashimura M, Hassamontr J, Dornfeld DA (1999) Effect of in-plane exit angle and rake angles on burr height and thickness in face milling operation. J Manuf Sci Eng 121(1):13–19
13. Horsch C, Schulze V, Lohe D (2006) Deburring and surface conditioning of micro milled structures by micro peening and ultrasonic wet peening. Microsyst Technol 12(7):691–696
14. Hoyle R (2008) Developments in micro and nano engineering and manufacturing. Plast Rubber Compos 37(2):50–56
15. Jaffery SI, Mativenga PT (2009) Assessment of the machinability of Ti-6Al-4 V alloy using the wear map approach. International Journal of Advance Manufacturing Technology 40:687–696
16. Jin X, Altintas Y (2011) Slip-line field model of micro-cutting process with round tool edge effect. J Mater Process Technol 211 (3):339–355
17. Jun MBG, Joshi SS, Devo RE, Kapoor SG (2008) An experimental evaluation of an atomization-based cutting fluid application system for micromachining. J Manuf Sci Eng 130(3):1–8
18. Karpat Y, Özel T (2007) Multi-objective optimization for turning processes using neural network modeling and dynamic-

neighborhood particle swarm optimization. Int J Adv Manuf Technol 35(3–4):234–247
19. Kennedy J, Eberhart RC (1995) Particle swarm optimization. Proc. IEEE Int. Conf. on Neural Networks, 4. IEEE Service Center, Piscataway, pp 1942–1948
20. Lee K, Dornfeld DA (2002) An experimental study on burr formation in micro milling aluminum and copper. Society of Manufacturing Engineers Technical Paper Series 30:1–8
21. Li H, Lai X, Li C, Feng J, Ni J (2008) Modelling and experimental analysis of the effects of tool wear, minimum chip thickness and micro tool geometry on the surface roughness in micro-end-milling. J Micromech Microeng 18(2):1–12
22. Liow JL (2009) Mechanical micromachining: a sustainable microdevice manufacturing approach. Journal of Clean Production 17 (7):662–667
23. Lu C (2008) Study on prediction of surface quality in machining process. J Mater Process Technol 205:439–450
24. Marcon A, Melkote S, Kalaitzidou K, DeBra D (2010) An experimental evaluation of graphite nanoplatelet based lubricant in micro-milling. CIRP Ann Manuf Technol 59(1):141–144
25. Masuzawa T (2000) State of the art of micromachining. CIRP Ann Manuf Technol 49(2):473–488
26. Mendes R, Kennedy J, Neves J (2004) The fully informed particle swarm: simpler, maybe better. IEEE Trans Evol Comput 8(3):204–210
27. Mian AJ, Driver N, Mativenga PT (2009) Micromachining of coarse-grained multi-phase material. Proceedings of the Institution of Mechanical Engineers. Journal of Engineering Manufacture: Part B 223(4):377–385
28. Montgomery DC (2005) Design and analysis of experiment. Wiley, Hoboken
29. Myers RH, Montgomery DC (2002) Response surface methodology: process and product optimization using designed experiments. Wiley, Hoboken
30. Özel T, Liu X (2009) Investigations on mechanics based process planning of micro-end milling in machining mold cavities. Mater Manuf Process 24:1274–1281
31. Özel T, Thepsonthi T, Ulutan D, Kaftanoğlu B (2011) Experiments and finite element simulations on micro-milling of Ti-6Al-4 V alloy with uncoated and cBN coated micro-tools, *CIRP* Annals-Manufacturing Technology, 60/2.
32. Park JB, Kim YK (2000) Metallic biomaterials. In: The biomedical engineering handbook, 2nd edn. CRC Press, Boca Raton
33. Ramsden JJ, Allen DM, Stephenson DJ, Alcock JR, Peggs GN, Fuller G, Goch G (2007) The design and manufacture of biomedical surfaces. CIRP Ann Manuf Technol 56(2):687–711
34. Schueler GM, Engmann J, Marx T, Haberland R, Aurich JC (2010) Burr formation and surface characteristics in micro-endmilling of titanium alloys. In: Burrs—analysis, control and removal. Springer, Berlin, pp 129–138
35. Shi Y, Eberhart RC (1998) Parameter selection in particle swarm optimization. Proc. Seventh Annual Conference on Evolutionary Programming, pp. 591–601.
36. Torres CD, Heaney PJ, Sumant AV, Hamilton MA, Carpick RW, Pfefferkorn FE (2009) Analyzing the performance of diamond-coated micro end mills. Int J Mach Tool Manuf 49:599–612
37. Vázquez E, Ciurana J, Rodríguez CA, Thepsonthi T, Özel T (2011) Swarm intelligent selection and optimization of machining system parameters for micro-channel fabrication in medical devices. Mater Manuf Process 26(3):403–414
38. Wang JS, Gong YD, Abba G, Chen K, Shi JS, Cai GQ (2008) Surface generation analysis in micro end-milling considering the influences of grain. Microsyst Technol 14(7):937–942
39. Wang W, Kweon SH, Yang SH (2005) A study on roughness of the micro-end-milled surface produced by a miniatured machine tool. Journal of Material Processing Technology 162–163:702–708
40. Weule H, Hüntrup V, Tritschler H (2001) Micro-cutting of steel to meet new requirements in miniaturization. CIRP Ann Manuf Technol 50(1):61–64